PROBING NONLINEARITY IN SUPERLATTICE HAFNIA-ZIRCONIA-ALUMINA NANOELECTROMECHANICAL RESONATORS

S M Enamul Hoque Yousuf, Troy Tharpe*, Roozbeh Tabrizian*, and Philip X.-L. Feng**
Department of Electrical and Computer Engineering, University of Florida, Gainesville, FL 32611, USA

ABSTRACT

We report on the nonlinearity in superlattice $Hf_{0.5}Zr_{0.5}O_2$-Al_2O_3 resonators, as probed by using optical interferometry, which demonstrates stiffening and softening nonlinearity, with 30nm-thick $Hf_{0.5}Zr_{0.5}O_2$ and 360nm-thick SiO_2 passivation layers, respectively. The $Hf_{0.5}Zr_{0.5}O_2$-Al_2O_3 resonator with 30nm $Hf_{0.5}Zr_{0.5}O_2$ passivation layer exhibits stiffening nonlinearity. However, in the resonator with 360nm SiO_2 passivation layer, the Duffing nonlinearity changes from stiffening to softening, thus providing a control knob to configure the nonlinearity in hafnia-zirconia-alumina superlattices. Therefore, by optimizing the layer thickness, the $Hf_{0.5}Zr_{0.5}O_2$-Al_2O_3-SiO_2 resonator can cancel these two types of nonlinearities and potentially offer a larger dynamic range. For the first time, we extract the Duffing coefficients $k_3 = 1.24\times10^5$ N/V^3 (30nm $Hf_{0.5}Zr_{0.5}O_2$ passivation) and -2.86×10^7 N/V^3 (360nm SiO_2 passivation). As such, $Hf_{0.5}Zr_{0.5}O_2$-Al_2O_3-SiO_2 resonators can be designed to operate in either linear or nonlinear regime by configuring relative layer thicknesses, enabling realization of CMOS compatible electromechanical clocks and new nonlinear resonators for emerging memory and computing architectures.

KEYWORDS

Nanoelectromechanical systems (NEMS), hafnia-zirconia-alumina, resonators, Duffing nonlinearity.

INTRODUCTION

Nanoelectromechanical systems (NEMS) couple the electrical and mechanical degrees of freedom and have enabled unique device applications, including sensors, actuators, signal processing and frequency control elements [1-3]. Ferroelectric hafnium dioxide (hafnia) can be combined with zirconia to form hafnia-zirconia ($Hf_xZr_{1-x}O_2$) which can be used to fabricate complementary metal oxide semiconductor (CMOS) compatible NEMS transducers. Hafnia-zirconia transducers are notable for their scalable fabrication via atomic layer deposition (ALD) and the ability to maintain robust polarization even at a thickness as low as 1nm, making them suitable for integrated high quality-factor (Q) NEMS resonators operating at high and very high frequencies [4]. It has been demonstrated that the integration of Al_2O_3 interlayers in hafnia-zirconia NEMS resonators forms a superlattice that sustains the ferroelectric properties and significantly enhances the energy density, resulting in high-Q NEMS resonators [3].

Superlattice hafnia-zirconia-alumina ($Hf_{0.5}Zr_{0.5}O_2$-Al_2O_3) nanoelectromechanical resonators fabricated using CMOS compatible technology can offer on-chip drive and readout schemes via efficient piezoelectric transduction. Thanks to the large electromechanical coupling, $Hf_{0.5}Zr_{0.5}O_2$-Al_2O_3 resonators can be driven into nonlinear regime, while the linear operational regime of the NEMS resonator is determined by the onset of nonlinearity. To realize standard functionality, a large linear range of operation is imperative and has been actively pursued in every signal domain. Dynamic range (DR), defined as the ratio between the highest non-distorted amplitude and the lowest detectable signal, is of paramount importance in signal transduction. Thus, a control knob to engineer the nonlinearity in NEMS resonators to enhance the DR leading to large linear operation regime is a long-sought quest in engineering [5]. Additionally, operating devices in nonlinear regime enables mode coupling and internal resonance, thus leading to rich dynamics that can be exploited in emerging device applications. Therefore, controllable nonlinearity in resonators is crucial to realize functionalities across the linear and nonlinear regimes.

In this digest paper, we report on the configurable nonlinearity in superlattice hafnia-zirconia-alumina NEMS resonators where the type of nonlinearity, *i.e.*, softening or hardening, can be controlled by the addition and control of silicon dioxide (SiO_2) content on the stack of superlattice layers constructing the resonator. We observe stiffening and softening nonlinearity with 30nm-thick $Hf_{0.5}Zr_{0.5}O_2$ and 360nm-thick SiO_2 passivation layers, respectively. We use an optical interferometry system to measure the nonlinear responses of the resonators and extract the Duffing (k_3) and quintic (k_5) nonlinear coefficients. Our experimental results show the potential of fabricating superlattice hafnia-zirconia-alumina NEMS resonators with optimized SiO_2 passivation layer thickness to counteract stiffening and softening nonlinearity, toward achieving large linear dynamic ranges of operations.

DEVICE DESIGN AND FABRICATION

Two port, clamped-clamped resonators transduced by superlattice $Hf_{0.5}Zr_{0.5}O_2$-Al_2O_3 with tungsten (W) electrodes are designed to excite the first-order flexural mode through three interdigitated transducers (IDTs). Resonators are designed with wide tethers and isolated ground planes to ensure optimal poling of $Hf_{0.5}Zr_{0.5}O_2$ and mitigate electrical feedthrough, respectively [1]. To investigate the impact of structural layer on nonlinear dynamics, superlattice resonators with identical dimensions of 44μm × 200μm, are fabricated and symmetrically encapsulated with either $Hf_{0.5}Zr_{0.5}O_2$ (Fig. 1a-1b), or SiO_2 (Fig. 1c-1d)), structural/ passivation layers. Both sets of resonators are fabricated following a previously reported, CMOS-compatible process [1], with additional SiO_2 deposition performed at 300ºC on an STS 310PC PECVD. Both sets of resonators are pulse-polled into the linear transduction regime through bipolar electric field cycling [1,6]. Figure 1b and 1d depicts cross-sectional transmission electron microscopy (XTEM) images of 30nm $Hf_{0.5}Zr_{0.5}O_2$ passivated and ~360nm SiO_2 passivated resonators, respectively. Figure 1e is an aerial view of scanning electron microscopy (SEM) image of a superlattice $Hf_{0.5}Zr_{0.5}O_2$-Al_2O_3 on SiO_2 resonator, highlighting the top side, isotropically etch-released from the host Si substrate.

RESONANCE CHARACTERIZATION

We measure the resonators using a custom-built optical interferometry system with a 633nm He-Ne laser (Fig. 2a) [7]. We use neutral-density filters to keep the laser power on the device below 65μW to avoid unwanted laser heating. We employ a 50× objective lens to maintain a laser spot size ~1μm. The laser is parked at the center of the suspended device to capture the out-of-plane fundamental mode and maximize the signal-to-background ratio (Fig. 2b). The device is mounted inside a vacuum chamber with hermetically sealed subminiature version A (SMA) connectors and optical window. We excite the device motion using piezoelectric transduction by applying a radio frequency (RF) voltage (v_{RF}) from a network analyzer to one of the electrodes through the SMA connector and grounding all the other ports (Fig. 2c). The reflected red laser from the resonator is modulated by the device motion,

978-1-940470-05-4/HH2024/$25©2024TRF
DOI 10.31438/TRF.HH2024.104

Solid-State Sensors, Actuators, and Microsystems Workshop
Hilton Head Island, South Carolina, 2-6 June 2024

converted to electrical signal by a photodetector and finally read out by the network analyzer (NA) [7]. The experiments are performed at room temperature with device in moderate vacuum (~20 mTorr).

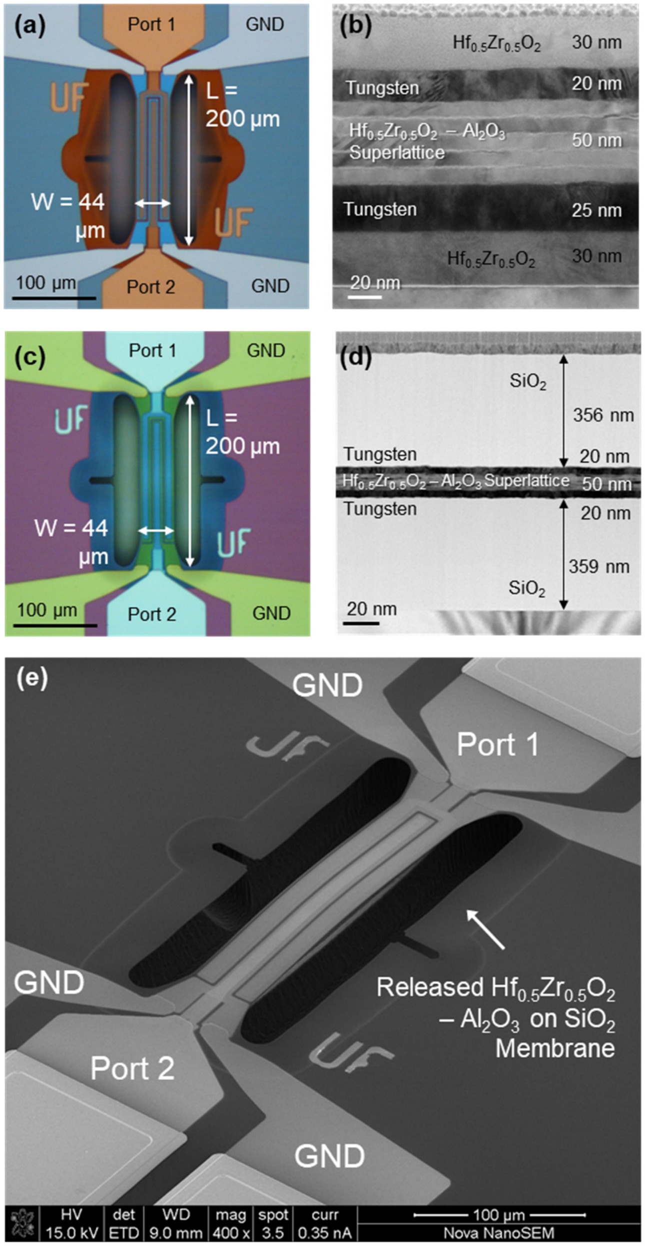

Figure 1: (a) Optical image of a two-port superlattice $Hf_{0.5}Zr_{0.5}O_2$-Al_2O_3 resonator with 30nm $Hf_{0.5}Zr_{0.5}O_2$ passivation. (b) X-TEM image of resonator in (a). (c) Optical image of a two port superlattice $Hf_{0.5}Zr_{0.5}O_2$-Al_2O_3 resonator with ~360nm SiO_2 passivation. (d) X-TEM image of resonator in (c). (e) Tilted view SEM image of a superlattice $Hf_{0.5}Zr_{0.5}O_2$-Al_2O_3-SiO_2 resonator, illustrating the top side of device released from substrate.

To characterize the resonators in the linear regime, we drive the devices with small v_{RF} = 10mV. From the measured responses of the devices, the resonance frequency (f_0) and quality factor (Q) can be extracted by fitting to a damped (finite-Q) harmonic resonator model. The resonator with 30nm $Hf_{0.5}Zr_{0.5}O_2$ passivation (Device 1) exhibits 1st flexural mode at f_0 =657kHz with Q = 3917 (Fig. 3a). The resonator with 360nm SiO_2 passivation layer (Device 2) exhibits the fundamental mode at f_0 =1.45MHz with Q = 2845 (Fig. 3b). Both devices demonstrate higher order modes; however, for nonlinearity measurements in this study, we focus on the fundamental mode of the resonators.

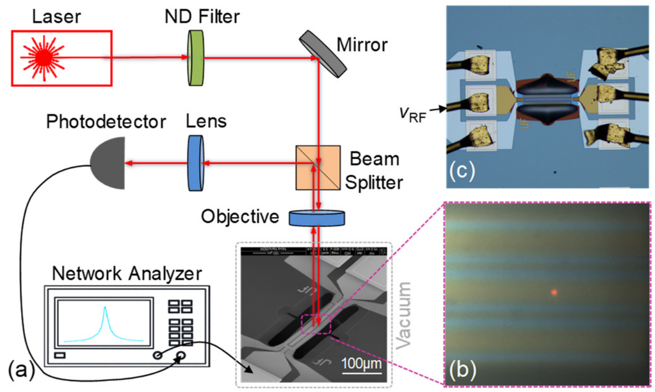

Figure 2: (a) Optical interferometry system for probing the response of the resonator. ND: neutral density. (b) Focused laser spot on the device during the measurement. (c) Optical microscopy image of the device after wire bonding, showing the input port (port 1, left) for exciting the device motion with v_{RF}. All the other ports are grounded.

DUFFING NONLINEARITY MEASUREMENT

To describe the motion of the resonator when we drive the device into nonlinearity by increasing v_{RF}, we consider a single degree of freedom system of a driven damped harmonic resonator with eigen frequency $\omega_0 = 2\pi f_0$, linear damping term ($\omega_0 \dot{x}/Q$), linear restoring force ($k_{eff}\, x = m_{eff}\, \omega_0^2 x$), Duffing nonlinearity ($k_3 x^3$), and quintic nonlinearity term ($k_5 x^5$). The governing equation for the motion of the resonator can be expressed as

$$m_{\mathrm{eff}}\ddot{x} + \frac{m_{\mathrm{eff}}\omega_0\dot{x}}{Q} + k_{\mathrm{eff}}x + k_3x^3 + k_5x^5 = F_{\mathrm{ext}} \qquad (1)$$

Here, m_{eff} is the effective mass of the resonator, k_3 and k_5 are Duffing and quintic nonlinear coefficients, and F_{ext}=Fcos(ωt) is the external driving force at angular frequency ω=2πf. The nonlinear stiffness components linked to k_3 and k_5 capture the amplitude dependent frequency shift at higher driving voltage and the concomitant bending of the frequency response curve near the resonance. By applying method of averaging to capture the slow variation of the amplitude and phase, the relationship between the instantaneous frequency (Ω) and amplitude (r) can be written as [8]

$$\Omega = \omega_0 + \frac{3k_3r^2}{8\omega_0 m_{\mathrm{eff}}} + \frac{5k_5r^4}{16\omega_0 m_{\mathrm{eff}}} \qquad (2)$$

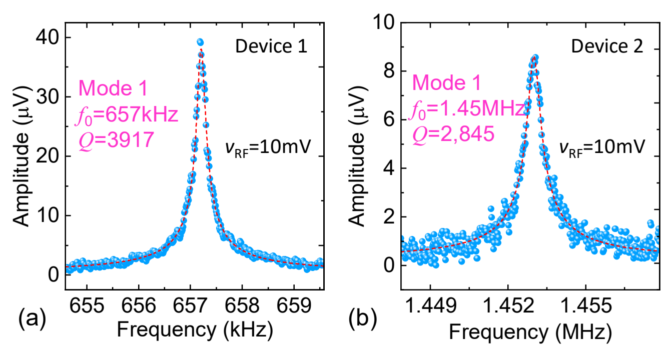

Figure 3: Measured fundamental flexural mode of $Hf_{0.5}Zr_{0.5}O_2$-Al_2O_3 resonators with (a) 30nm $Hf_{0.5}Zr_{0.5}O_2$ and (b) 360nm SiO_2 passivation. Blue spheres are measured data, and dashed red curves are fitting to the finite-Q harmonic resonator model.

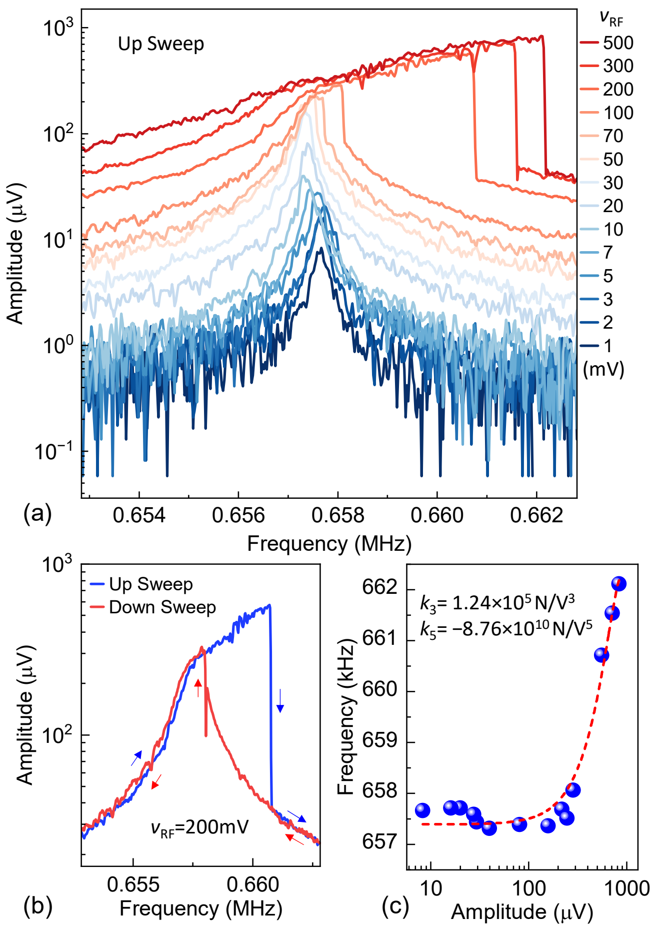

Figure 4: (a) Measured driven resonance response of a $Hf_{0.5}Zr_{0.5}O_2$-Al_2O_3 resonator with 30nm $Hf_{0.5}Zr_{0.5}O_2$ passivation layer at varying v_{RF} from 1mV to 500mV. The response is recorded during sweeping up the drive frequency. (b) Frequency hysteresis during up and down frequency sweeps at v_{RF} =200mV. (c) Resonance frequency versus amplitude (backbone curve). Blue data points are extracted from (a), and red dashed line represents a fit to Eq. (2).

Here, Eq. (2) describes the backbone curve of the nonlinear response of the resonator at higher amplitude and can be used to estimate the stiffness parameters k_3 and k_5 from experimentally measured results as fitting parameters (Fig. 4c, note x and r are in voltage domain).

We drive the resonators into nonlinearity by increasing v_{RF} to higher drive voltage and measure the response optically using the optical interferometry system. The resonance frequency increases in the resonator with 30nm $Hf_{0.5}Zr_{0.5}O_2$ passivation as we increase drive voltage v_{RF} from 1mV to 500mV (Fig. 4a). This indicates that the stiffening nonlinearity demonstrates in this resonator (Device 1) with increasing RF voltage.

In a Duffing resonator, for drive level above the critical drive $v_{RF,c}$, there are certain frequencies at which three values in amplitude are possible. From stability analysis, among these three amplitudes, one of the solutions is unstable and the other two are stable. A trace of such stable solutions at various given frequencies leads to an upper and lower stable branch. While the unstable branch is not accessible during the frequency domain measurement using a network analyzer, the two stable branches can be accessed depending on the frequency sweep direction, and thus give rise to bistability in Duffing resonators. Therefore, depending on the direction of the frequency sweep, the resonance response is different and causes a frequency hysteresis in the resonator response. The jump in the amplitude response occurs at the saddle-nodes of the resonator response. Figure 4b shows such frequency hysteresis observed in the resonator with 30nm $Hf_{0.5}Zr_{0.5}O_2$ passivation with v_{RF} = 200mV. During the up sweep, the amplitude jumps from the upper stable branch to the lower stable branch at f_u = 0.660690MHz, whereas during the down sweep, the amplitude jumps from the lower stable branch to the upper stable branch at f_d = 0.657865MHz. The frequency hysteresis during up and down frequency sweep is ~2.825kHz. The frequency hysteresis increases with higher driving force. If we keep decreasing the driving force, the two saddle nodes corresponding to the amplitude jumps from upper to lower and lower to upper stable branches become identical. This point, called critical amplitude (a_c), defines the threshold for the resonator response to become nonlinear. We can calibrate the motion in the displacement domain and calculate the corresponding critical amplitude a_c. From our measured results, the readout voltage corresponding to the critical amplitude is ~217µV at a drive level of $v_{RF,c}$ ~ 70mV.

To quantify the Duffing and quintic nonlinearity, we extract the frequencies and amplitudes corresponding to the saddle nodes during up sweep. We then plot the resonance frequency versus amplitude of the mode as shown in Fig. 4c. The red dashed line is a fit to experimental data using Eq. (2). For fitting the data, we keep the linear resonance frequency ω_0 = 0.657MHz, m_{eff} = 6.01×10^{-12} kg as constants. Then we perform the fitting and obtain a Duffing coefficient k_3 = 1.24×10^5 N/V^3 and a quintic nonlinear coefficient k_5 = -8.76×10^{10} N/V^5 (note x and r are in voltage). The positive Duffing coefficient indicates stiffening nonlinearity in Device 1.

Next, we test the $Hf_{0.5}Zr_{0.5}O_2$-Al_2O_3 resonator with 360nm SiO_2 passivation at higher driving voltage. Figure 5a shows the measured responses as we increase v_{RF} from 1mV to 200mV. The resonator frequency decreases as we increase the driving force. This indicates that the resonator demonstrates softening nonlinearity. To observe the frequency hysteresis, we drive the device into nonlinear regime with v_{RF} = 100mV and measure both up and down sweeps (Fig. 5b). During the down sweep, the amplitude jumps from the upper stable branch to the lower stable branch at f_d = 1.45005MHz, whereas during the up sweep, the amplitude jumps from the lower stable branch to the upper stable branch at f_u = 1.4521MHz. Thus, this device demonstrates ~2.05kHz frequency hysteresis during up and down sweep at v_{RF} = 100mV. With higher drive voltage, the frequency hysteresis increases. To evaluate the Duffing and quintic nonlinear coefficients, we extract the frequencies and amplitudes corresponding to the saddle nodes during down sweep. We then plot the resonance frequency versus amplitude of the mode as shown in Fig. 5c. The red dashed line is a fit to experimental data using Eq. (2). For fitting the data, we keep the linear resonance frequency ω_0 = 1.45MHz, m_{eff} = 9.86×10^{-12} kg as constants. We then perform the fitting and obtain Duffing coefficient k_3 = -2.86×10^7 N/V^3 and quintic nonlinear coefficient k_5 = 1.36×10^{15} N/V^5. The negative Duffing coefficient indicates the softening nonlinearity in the resonator. Table 1 summarizes all the measured and extracted parameters from the $Hf_{0.5}Zr_{0.5}O_2$-Al_2O_3 resonators with 30nm $Hf_{0.5}Zr_{0.5}O_2$ passivation and with 360nm SiO_2 passivation.

$Hf_{0.5}Zr_{0.5}O_2$-Al_2O_3 resonator with 30nm $Hf_{0.5}Zr_{0.5}O_2$ passivation shows stiffening nonlinearity, whereas $Hf_{0.5}Zr_{0.5}O_2$-Al_2O_3 resonator with 360nm SiO_2 passivation layer exhibits softening nonlinearity. Therefore, by controlling the thickness of SiO_2 (likely <360nm) in the resonator, it could be possible to realize a resonator where stiffening and softening nonlinearity cancel each other, and the onset of nonlinearity is higher compared to the $Hf_{0.5}Zr_{0.5}O_2$-Al_2O_3 resonator with 30nm $Hf_{0.5}Zr_{0.5}O_2$ passivation.

Thus, we predict 1st order flexural mode in hafnia-zirconia-alumina superlattice with large linear range of operation with optimized SiO_2 layer thickness, leading to a large dynamic range. Moreover, $Hf_{0.5}Zr_{0.5}O_2$-Al_2O_3 resonators can be designed to operate both in stiffening and softening Duffing nonlinearity depending on the designed passivation layer. Thus, our results pave the way for studying nonlinearity in ferroelectric $Hf_{0.5}Zr_{0.5}O_2$-Al_2O_3 resonators for emerging applications.

Table 1: Summary of the measured responses from the fabricated $Hf_{0.5}Zr_{0.5}O_2$-Al_2O_3 resonators.

Parameters	Device 1	Device 2
Passivation Layer	30nm $Hf_{0.5}Zr_{0.5}O_2$	360nm SiO_2
f_0 (MHz)	0.66	1.45
Measured Q	3917	2845
$v_{RF,c}$ (mV)	~70	~50
k_3 (N/V^3)	1.24×10^5	-2.86×10^7
k_5 (N/V^5)	-8.76×10^{10}	1.36×10^{15}

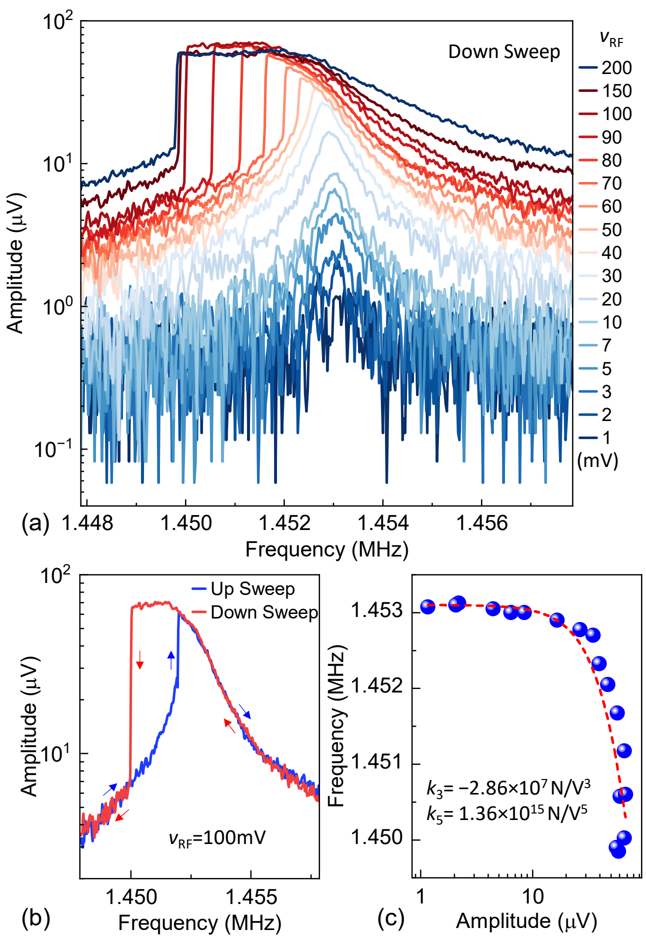

Figure 5: (a) Driven resonance of $Hf_{0.5}Zr_{0.5}O_2$-Al_2O_3 resonator with 360nm SiO_2 passivation at varying v_{RF} from 1mV to 200mV showing softening nonlinearity. (b) Frequency hysteresis due to up and down frequency sweeps. (c) Resonance frequency versus amplitude (backbone curve). Blue data points are extracted from (a), and the red dashed line represents a fitting curve to Eq. (2).

CONCLUSION

In summary, we have demonstrated superlattice hafnia-zirconia-alumina ($Hf_{0.5}Zr_{0.5}O_2$-Al_2O_3) NEMS resonators with 30nm-thick $Hf_{0.5}Zr_{0.5}O_2$ and 360nm-thick SiO_2 passivation layer and measured the nonlinearity to identify and characterize the types of nonlinear responses. The NEMS resonator with 30nm-thick $Hf_{0.5}Zr_{0.5}O_2$ passivation (Device 1) demonstrates stiffening nonlinearity, whereas the resonator with 360nm SiO_2 passivation (Device 2) exhibits softening nonlinearity. Therefore, $Hf_{0.5}Zr_{0.5}O_2$-Al_2O_3 resonators are suitable candidates for nonlinear device applications where the nonlinearity can be configured by controlling the passivation SiO_2 thickness. We also envision NEMS resonators with optimized SiO_2 passivation layer with large linear range of operation for various frequency control applications.

ACKNOWLEDGEMENTS

The authors would like to thank the staff at the Nanoscale Research Facility (NRF) at University of Florida (UF) for their technical support on device fabrication. We thank the funding from NSF through grants DUE-2142552, OSI-2326528, and ECCS-1752206, and DARPA through the YFA program.

REFERENCES

[1] T. Tharpe, E. Hershkovitz, F. Hakim, H. Kim, and R. Tabrizian, "Nanoelectromechanical resonators for gigahertz frequency control based on hafnia–zirconia–alumina superlattices", *Nat. Electron.*, vol. 6, no. 8, pp. 599-609, 2023. doi: 10.1038/s41928-023-00999-9.

[2] S M E. H. Yousuf and P. X.-L. Feng, "Atomic layer self-transducing MoS_2 vibrating channel transistors with 0.5 pm/Hz$^{1/2}$ displacement sensitivity at room temperature", *Appl. Phys. Lett.*, vol. 124, no. 5, art. no. 53503, 2024. doi: 10.1063/5.0170127/3253550.

[3] X.-Q. Zheng, T. Tharpe, S M E. H. Yousuf, N. G. Rudawski, P. X.-L. Feng, and R. Tabrizian, "High quality factors in superlattice ferroelectric $Hf_{0.5}Zr_{0.5}O_2$ nanoelectromechanical resonators", *ACS Appl. Mater. Interfaces*, vol. 14, no. 32, pp. 36807-36814, 2022. doi: 10.1021/acsami.2c08414.

[4] M. Ghatge, G. Walters, T. Nishida, and R. Tabrizian, "An ultrathin integrated nanoelectromechanical transducer based on hafnium zirconium oxide", *Nat. Electron.*, vol. 2, no. 11, pp. 506-512, 2019. doi: 10.1038/s41928-019-0305-3.

[5] J. Lee, Z. Wang, K. He, R. Yang, J. Shan, and P. X.-L. Feng, "Electrically tunable single- and few-layer MoS_2 nanoelectromechanical systems with broad dynamic range", *Sci. Adv.*, vol. 4, no. 3, art. no. eaao6653, 2018. doi: 10.1126/sciadv.aao6653.

[6] M. Lederer, *et al.*, "On the origin of wake-up and antiferroelectric-like behavior in ferroelectric hafnium oxide", *Phys. Status Solidi (RRL) – Rapid Res. Lett.*, vol. 15, no. 5, art. no. 2100086, 2021. doi: 10.1002/PSSR.202100086.

[7] S M E. H. Yousuf, J. Lee, S. W. Shaw, and P. X.-L. Feng, "Phononic frequency combs in atomically thin nanoelectromechanical resonators via 1:1 and 2:1 internal resonances", *J. Microelectromech. Syst.*, vol. 32, no. 4, pp. 335-346, 2023. doi: 10.1109/JMEMS.2023.3282233.

[8] T. Kaisar, J. Lee, D. Li, S. W. Shaw, and P. X.-L. Feng, "Nonlinear stiffness and nonlinear damping in atomically thin MoS_2 nanomechanical resonators", *Nano Lett.*, vol. 22, no. 24, pp. 9831-9838, 2022. doi: 10.1021/acs.nanolett.3c02691.

CONTACT

*S M Enamul Hoque Yousuf: syousuf@ufl.edu
*Troy Tharpe: troytharpe@gmail.com
*Roozbeh Tabrizian: rtabrizian@ece.ufl.edu
*Philip Feng: philip.feng@ufl.edu